



This discussion paper is/has been under review for the journal Geoscientific Model Development (GMD). Please refer to the corresponding final paper in GMD if available.

LOSCAR: Long-term Ocean-atmosphere-Sediment Carbon cycle Reservoir Model

R. E. Zeebe

School of Ocean and Earth Science and Technology, University of Hawaii at Manoa, 1000
Pope Road, MSB 504, Honolulu, 96822, USA

Received: 24 May 2011 – Accepted: 14 June 2011 – Published: 29 June 2011

Correspondence to: R. E. Zeebe (zeebe@soest.hawaii.edu)

Published by Copernicus Publications on behalf of the European Geosciences Union.

[Title Page](#)

[Abstract](#)

[Introduction](#)

[Conclusions](#)

[References](#)

[Tables](#)

[Figures](#)



[Back](#)

[Close](#)

[Full Screen / Esc](#)

[Printer-friendly Version](#)

[Interactive Discussion](#)



Abstract

The LOSCAR model is designed to efficiently compute the partitioning of carbon between ocean, atmosphere, and sediments on time scales ranging from centuries to millions of years. While a variety of computationally inexpensive carbon cycle models are already available, many are missing a critical sediment component, which is indispensable for long-term integrations. One of LOSCAR's strengths is the coupling of ocean-atmosphere routines to a computationally efficient sediment module. This allows, for instance, adequate computation of CaCO_3 dissolution, calcite compensation, and long-term carbon cycle fluxes, including weathering of carbonate and silicate rocks. The ocean component includes various biogeochemical tracers such as total carbon, alkalinity, phosphate, oxygen, and stable carbon isotopes. We have previously published applications of the model tackling future projections of ocean chemistry and weathering, $p\text{CO}_2$ sensitivity to carbon cycle perturbations throughout the Cenozoic, and carbon/calcium cycling during the Paleocene-Eocene Thermal Maximum. The focus of the present contribution is the detailed description of the model including numerical architecture, processes and parameterizations, tuning, and examples of input and output. Typical CPU integration times of LOSCAR are of order seconds for several thousand model years on current standard desktop machines. The LOSCAR source code in C can be obtained from the author by sending a request to loscar.model@gmail.com.

1 Introduction

Various carbon cycle models that are computationally inexpensive have been developed in the past, in particular box models of the ocean's carbon cycle (e.g. Sarmiento and Toggweiler, 1984; Walker and Kasting, 1992; Toggweiler, 1999; Munhoven and Francois, 1996; Köhler et al., 2005). However, only a few studies have considered sediments (e.g. Sundquist, 1986; Sigman et al., 1998; Ridgwell, 2001) and included

GMDD

4, 1435–1476, 2011

LOSCAR

R. E. Zeebe

Title Page

Abstract

Introduction

Conclusions

References

Tables

Figures

◀

▶

◀

▶

Back

Close

Full Screen / Esc

Printer-friendly Version

Interactive Discussion



LOSCAR

R. E. Zeebe

[Title Page](#)[Abstract](#)[Introduction](#)[Conclusions](#)[References](#)[Tables](#)[Figures](#)[Back](#)[Close](#)[Full Screen / Esc](#)[Printer-friendly Version](#)[Interactive Discussion](#)

long-term carbon cycle fluxes such as carbonate and silicate rock weathering (e.g. Shaffer et al., 2008). The LOSCAR model (Long-term Ocean-atmosphere-Sediment CARbon cycle Reservoir model) closes this gap. LOSCAR is primarily designed to efficiently compute the partitioning of carbon between ocean, atmosphere, and sediments on time scales ranging from centuries to millions of years. LOSCAR includes various biogeochemical tracers such as total dissolved inorganic carbon (TCO₂), total alkalinity (TA), phosphate (PO₄), oxygen (O₂), stable carbon isotopes ($\delta^{13}\text{C}$), and %CaCO₃ in sediments. Based on the predicted tracer distributions, different variables are computed including atmospheric CO₂, ocean pH, calcite and aragonite saturation state, calcite compensation depth (CCD) and more. LOSCAR also allows for changes in the major ion composition of seawater, including the seawater Mg/Ca ratio, which is critical for paleo-applications. The major ion seawater composition affects thermodynamic quantities such as equilibrium constants and solubility products, which in turn affect the predicted ocean carbonate chemistry and atmospheric CO₂.

We have previously published several applications of LOSCAR dealing, for instance, with future projections of ocean chemistry and weathering, $p\text{CO}_2$ sensitivity to carbon cycle perturbations throughout the Cenozoic, and carbon/calcium cycling during the Paleocene-Eocene Thermal Maximum (PETM) (Zeebe et al., 2008, 2009; Uchikawa and Zeebe, 2008; Stuecker and Zeebe, 2010; Uchikawa and Zeebe, 2010; Komar and Zeebe, 2011; Zeebe and Ridgwell, 2011). The subject of the present contribution is the detailed description of the model including numerical architecture, processes and parameterizations, tuning, and examples of input and output. It may appear that publishing model applications before a detailed model description is putting the cart before the horse. One of the reasons for this is that the journals interested in publishing the model applications have little or no interest in publishing a detailed model description. Journals that provide a forum for technical model descriptions are rare, and so the recent appearance of *Geoscientific Model Development* has encouraged me to provide a coherent model description of LOSCAR that will hopefully be useful for the readership of the journal, as well as the users of the model. On the other hand, publishing a

few model applications before the detailed model description also has an advantage. LOSCAR, for example, has been extensively tested by now and several bugs and scientific/numerical issues have already been fixed.

LOSCAR's main components include ocean, atmosphere, and marine sediments.

5 The model architecture, main components, model variables, and process parameterizations will be described in the following. Finally, two input/output examples will be presented, one dealing with anthropogenic fossil fuel emissions, the other with carbon release during the PETM.

2 Architecture

10 The basic architecture of the model is fairly simple. For all model variables y_i , i.e. all tracers in all compartments (atmosphere, ocean boxes, and sediment boxes), a system of coupled, first-order ordinary differential equations is solved:

$$\frac{dy_i}{dt} = F(t, y_1, y_2, \dots, y_{\text{NEQ}}), \quad (1)$$

where t is time, NEQ is the total number of equations, $i = 1, 2, \dots, \text{NEQ}$, and F 's are known functions. Note that for most applications, the derivatives (right-hand side of Eq. 1) do not explicitly depend on the independent variable t . For given start (initial) conditions \mathbf{y}_0 at t_{start} , the equations are then integrated forward in time over the interval from t_{start} to t_{final} . Standard numerical procedures (solvers) for this sort of problem are available. One thing to keep in mind is that the equations solved in LOSCAR are typically stiff and involve different time scales, which requires a solver for stiff problems with adaptive stepsize control. The solver implemented in the C version of LOSCAR is a fourth-order Rosenbrock method with automatic stepsize adjustment (Press et al., 20 1992).

25 Once the initial conditions \mathbf{y}_0 and derivatives F 's have been supplied, the solution of the problem is usually straightforward. However, setting up \mathbf{y}_0 and F requires some

Title Page

Abstract

Introduction

Conclusions

References

Tables

Figures



Back

Close

Full Screen / Esc

Printer-friendly Version

Interactive Discussion



work. In the following, the individual model components will be described and expressions will be given for individual F 's that enter Eq. (1). The current setup includes two different model versions: a “modern” version and a Paleocene/Eocene version (“P/E”-version for short).

3 Ocean

3.1 Geometry

The global ocean is geometrically divided in LOSCAR into separate ocean basins representing Atlantic, Indian, and Pacific Ocean (plus Tethys in the P/E-version). In turn, each ocean basin is subdivided into surface, intermediate, and deep ocean (Fig. 1). In addition, the model includes a generic high-latitude box (H-box), representing cold surface waters without reference to a specific location (cf. Walker and Kasting, 1992; Toggweiler, 1999). As a result, the total number of ocean boxes is $NB = 10$ in the modern version and $NB = 13$ in the P/E-version. Box areas and volumes are given in Table 1. The modern ocean geometry in LOSCAR is not unlike the one used by Walker and Kasting (1992). However, Walker and Kasting (1992) combined the warm surface and thermocline waters each into a single reservoir for a total of 6 boxes to represent the global modern ocean.

The modern and Paleocene/Eocene ocean bathymetry in LOSCAR is based on Menard and Smith (1966) and Bice and Marotzke (2002), respectively. The bathymetry determines the surface area and volume of ocean boxes (Table 1) and the surface area-depth level relationship of the sediment boxes (Sect. 6).

3.2 Ocean tracer equations

Let y_k be a subset of \mathbf{y} (Eq. 1), representing ocean tracer variables including TCO_2 , TA , PO_4 , etc. (in this particular order). Then $k = 1, 2, \dots, NB$ for TCO_2 , $k = NB + 1, NB +$

GMDD

4, 1435–1476, 2011

LOSCAR

R. E. Zeebe

Title Page

Abstract

Introduction

Conclusions

References

Tables

Figures

◀

▶

◀

▶

Back

Close

Full Screen / Esc

Printer-friendly Version

Interactive Discussion



2, ..., 2NB for TA, $k = 2NB + 1, 2NB + 2, \dots, 3NB$ for PO_4 , and so on. If the total number of ocean tracers is NOCT, then the total number of equations for all ocean tracers and boxes is NOCT \times NB. The differential equation for an ocean tracer y_k may be written in the general form:

$$5 \quad V_k \frac{dy_k}{dt} = F_{\text{thm}} + F_{\text{gas}} + F_{\text{bio}} + F_{\text{in}} + F_{\text{sed}}, \quad (2)$$

where V_k is the volume of box k and F 's are fluxes due to (thermohaline) circulation and mixing, air-sea gas exchange (e.g. in case of TCO_2), biological uptake and remineralization, riverine/weathering input, and sediment fluxes. The first three flux terms on the right-hand side of Eq. (2) will be explained in the following subsections; the riverine/weathering and sediment flux terms will be explained in Sects. 4 and 6.

3.2.1 Circulation, mixing, and air-sea gas exchange

Given a prescribed ocean circulation- and mixing scheme, F_{thm} is of the form:

$$15 \quad V_k \left(\frac{dy_k}{dt} \right)_{\text{thm}} = T \sum (y_j - y_k) + m_{lk} \sum (y_l - y_k) \quad (3)$$

where T is the volume transport of the conveyor circulation and m_{lk} are mixing coefficients between boxes l and k (Fig. 2, Table 2). The box indices j and l are set by the prescribed circulation/mixing scheme (Fig. 2). The coefficients m_{lk} represent bidirectional mixing, hence $m_{lk} = m_{kl}$.

The air-sea gas exchange term reads:

Title Page

Abstract

Introduction

Conclusions

References

Tables

Figures



Back

Close

Full Screen / Esc

Printer-friendly Version

Interactive Discussion



$$V_k \left(\frac{dy_k}{dt} \right)_{\text{gas}} = \kappa_{\text{as}} A_k (p\text{CO}_2^a - P\text{CO}_2^k) \quad (4)$$

where κ_{as} is the air-sea gas exchange coefficient for CO_2 and A_k is the area of surface box k ; $p\text{CO}_2^a$ and $P\text{CO}_2^k$ is the atmospheric $p\text{CO}_2$ and the $p\text{CO}_2$ in equilibrium with dissolved CO_2 in surface box k , respectively. The index k runs over all surface boxes and for tracers such as TCO_2 and T^{13}CO_2 .

3.2.2 Biological pump

The biological uptake and recycling of tracers is parameterized based on phosphate (PO_4 for short). For instance, net uptake of PO_4 in the low-latitude surface ocean (equivalent to particle export flux from the mixed layer) is calculated as:

$$V_k \left(\frac{d[\text{PO}_4]_k}{dt} \right)_{\text{upt}} = F_{\text{ppl}}^k = -f_{\text{epI}} m_{jk} [\text{PO}_4]_j, \quad (5)$$

where the parameter f_{epI} describes the efficiency for PO_4 uptake in the low-latitude surface boxes, $m_{jk} \times [\text{PO}_4]_j$ is the flux of PO_4 supplied by upwelling/mixing from the underlying intermediate box j into the surface box k . (Note that in the model, the conveyor transport T does not directly supply nutrients to the warm surface waters; it does so, however, to the cold surface waters, see Fig. 2). If f_{epI} were to approach 1.0 (100% efficiency), all upwelled PO_4 would be converted to sinking particles and the phosphate concentration of surface box k would be zero. In the model, as well as in reality, f_{epI} is usually less than 1.0 (Table 2). The fraction f_{rim} of the export flux is remineralized in the intermediate box, whereas the fraction $(1 - f_{\text{rim}})$ is remineralized in the deep box.

The high-latitude PO_4 export flux can be set directly by assigning a value to the flux parameter F_{pph} . If the value chosen is too large to be supported by the total PO_4

Title Page

Abstract

Introduction

Conclusions

References

Tables

Figures



Back

Close

Full Screen / Esc

Printer-friendly Version

Interactive Discussion



influx entering the H-box, simple Michaelis-Menten kinetics prevent PO_4 from becoming negative. Caution is therefore advised when increasing F_{pph} because the actual high-latitude export flux may be less than the value assigned to F_{pph} . The high-latitude export flux is remineralized in the deep boxes.

The fluxes of TCO_2 and TA due to biological uptake and recycling are computed based on PO_4 using a given Redfield- and rain ratio (Table 2). Note that there is a small contribution to alkalinity changes from organic carbon production and respiration as a result of nitrate uptake and release (e.g. Zeebe and Wolf-Gladrow, 2001). The major contribution to alkalinity changes in the model is associated with CaCO_3 fluxes. Of the total CaCO_3 export flux, the larger fraction is destined for accumulation or dissolution in sediments, the latter of which returns total carbon and alkalinity to the ocean (Sect. 6). A smaller fraction of the CaCO_3 export is assumed to dissolve in the water column (Table 2). This assumption yields better agreement with observed TA fields and is consistent with observations and modeling studies indicating substantial water column dissolution above the lysocline (e.g. Archer et al., 1998; Milliman et al., 1999; Feely et al., 2002).

4 Carbonate and silicate weathering

Weathering of carbonate rocks on the continents takes up atmospheric CO_2 and supplies calcium and bicarbonate ions to the ocean:



Hence two moles of carbon and one mole of Ca^{2+} enter the ocean for each mole of CaCO_3 weathered, raising ocean TCO_2 and TA by two units each (Fig. 3). If the CaCO_3 riverine/weathering influx is denoted by F_{cc} (in units of $\text{mol CaCO}_3 \text{ y}^{-1}$, see Table 3), then:

Title Page

Abstract

Introduction

Conclusions

References

Tables

Figures



Back

Close

Full Screen / Esc

Printer-friendly Version

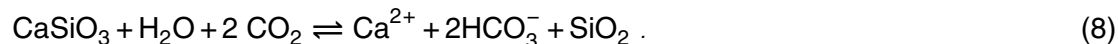
Interactive Discussion



$$V_k \left(\frac{d[\text{TCO}_2]_k}{dt} \right)_{\text{cc}} = V_k \left(\frac{d[\text{TA}]_k}{dt} \right)_{\text{cc}} = 2 F_{\text{cc}} \text{NOC}^{-1} \quad (7)$$

where $k = 1, \dots, \text{NOC}$ runs over all low-latitude surface boxes and NOC is the number of corresponding ocean basins. Note that in steady state, subsequent precipitation of CaCO_3 in the ocean (Reaction 6 backwards) releases the same amount of CO_2 back into the atmosphere as was taken up during weathering. In other words, the CO_2 for carbonate weathering essentially originates from the ocean (Fig. 3). As a result, although the addition of Ca^{2+} and 2HCO_3^- increases ocean $\text{TCO}_2 : \text{TA}$ in a 2:2 ratio, on a net basis CaCO_3 weathering increases ocean $\text{TCO}_2 : \text{TA}$ in a 1:2 ratio because one mole of CO_2 returns to the atmosphere. If influx equals burial, carbonate weathering thus represents a zero net balance for atmospheric CO_2 . The steady-state balance is restored after a perturbation on a time scale of 5 to 10 ky and is referred to as “calcite compensation” (Broecker and Peng, 1987; Zeebe and Westbroek, 2003).

Weathering of silicate rocks and simultaneous uptake of atmospheric CO_2 may be described by:



If the CaSiO_3 riverine/weathering influx is denoted by F_{si} (in units of $\text{mol CaSiO}_3 \text{y}^{-1}$, see Table 3), then:

$$V_k \left(\frac{d[\text{TCO}_2]_k}{dt} \right)_{\text{si}} = V_k \left(\frac{d[\text{TA}]_k}{dt} \right)_{\text{si}} = 2 F_{\text{si}} \text{NOC}^{-1} \quad (9)$$

Note that silicate weathering removes 2 moles of CO_2 from the atmosphere for each mole of CaSiO_3 weathered. Subsequent precipitation and burial of CaCO_3 (Reaction 6 backwards) releases one mole of CO_2 back to the atmosphere, the other mole is buried in the form of CaCO_3 in sediments (Fig. 3). In steady state, the balance is closed by long-term CO_2 input to the atmosphere from volcanic degassing. Putting it the other

[Title Page](#)[Abstract](#)[Introduction](#)[Conclusions](#)[References](#)[Tables](#)[Figures](#)[Back](#)[Close](#)[Full Screen / Esc](#)[Printer-friendly Version](#)[Interactive Discussion](#)

way, the CO₂ released by volcanoes is balanced by silicate weathering and subsequent carbonate burial in the ocean (Fig. 3). The net reaction is:



The steady-state balance for silicate weathering is restored after a perturbation on a time scale of 10⁵ to 10⁶ yr. This process also restores the partial pressure of atmospheric CO₂ in order to maintain a mass balance of long-term carbon cycle fluxes (e.g. Berner et al., 1983; Zeebe and Caldeira, 2008).

The restoring time scale for silicate weathering is much longer than for carbonate weathering for two reasons. First, silicate weathering requires whole-ocean TCO₂ to adjust, whereas carbonate weathering only requires the ocean's carbonate ion concentration to adjust. On average, the modern TCO₂ inventory is about 20 times larger than mean-ocean [CO₃²⁻]. Second, carbonate weathering fluxes have been estimated to be about 2.5-times larger than silicate weathering fluxes (Table 3). Combined, this gives a factor of about 50, which, multiplied by the calcite compensation time scale of 10 ky, gives 500 ky, which is about right.

4.1 Weathering feedback

The feedback between atmospheric CO₂ and weathering fluxes of carbonates and silicates is parameterized in the model using the following equations (see Walker et al., 1981; Berner et al., 1983; Walker and Kasting, 1992):

$$F_{\text{cc}} = F_{\text{cc}}^0 \left(p\text{CO}_2 / p\text{CO}_2^0 \right)^{n_{\text{cc}}} \quad (11)$$

$$F_{\text{si}} = F_{\text{si}}^0 \left(p\text{CO}_2 / p\text{CO}_2^0 \right)^{n_{\text{si}}} \quad (12)$$

where the superscript “0” refers to the initial (steady-state) value of the weathering flux and pCO₂, respectively. The parameters n_{cc} and n_{si} control the strength of the weathering feedback (Table 3). For a detailed discussion of the uncertainties associated

Title Page

Abstract

Introduction

Conclusions

References

Tables

Figures



Back

Close

Full Screen / Esc

Printer-friendly Version

Interactive Discussion



with the weathering parameterization, see Uchikawa and Zeebe (2008). As mentioned above, in steady state, the silicate weathering flux balances the CO₂ degassing flux from volcanism:

$$F_{\text{si}}^0 = F_{\text{vc}}^0 \quad (13)$$

5 Thus, the long-term steady-state $p\text{CO}_2$ of the model is set by picking a value for $p\text{CO}_2^0$, which drives the system towards equilibrium via the silicate weathering equation (Eq. 12). Only when the actual model $p\text{CO}_2$ equals $p\text{CO}_2^0$, will the fluxes be balanced ($F_{\text{si}} = F_{\text{si}}^0 = F_{\text{vc}}^0$).

5 Atmosphere

10 The model variable tracking the inventory of atmospheric carbon dioxide, C_{atm} , is related to the partial pressure of CO₂ in the atmosphere by:

$$C_{\text{atm}} = p\text{CO}_2^a \times q^0 \quad (14)$$

where $q^0 = (2.2 \times 10^{15} / 12) \text{ mol ppmv}^{-1}$ converts from ppmv to mol. Note that for numerical scaling purposes (see Sect. 7.4), C_{atm} is normalized to order 1 in the program
 15 by multiplying by $(A_{\text{oc}} \times 100)^{-1}$ (arbitrary factor). The differential equation for C_{atm} may be written in the general form (an analogous equation holds for $^{13}\text{C}_{\text{atm}}$):

$$\frac{d C_{\text{atm}}}{dt} = F_{\text{gas}} + F_{\text{vc}} - F_{\text{cc}} - 2 F_{\text{si}} + C_{\text{in}}, \quad (15)$$

where F 's are fluxes due to air-sea gas exchange, volcanic input and weathering (see Sect. 4), and possible carbon input sources. The air-sea gas exchange term for the
 20 atmosphere reads:

Title Page

Abstract

Introduction

Conclusions

References

Tables

Figures



Back

Close

Full Screen / Esc

Printer-friendly Version

Interactive Discussion



$$\left(\frac{d C_{\text{atm}}}{dt}\right)_{\text{gas}} = \sum \kappa_{\text{as}} A_k (P\text{CO}_2^k - p\text{CO}_2^a) \quad (16)$$

where κ_{as} is the air-sea gas exchange coefficient for CO_2 and A_k is the area of surface box k ; $p\text{CO}_2^a$ and $P\text{CO}_2^k$ is the atmospheric $p\text{CO}_2$ and the $p\text{CO}_2$ in equilibrium with dissolved CO_2 in surface box k , respectively. The sum runs over all surface boxes. In case of carbon input to the atmosphere from fossil fuel burning or from other carbon sources, for instance, during the PETM, a term of the form:

$$\left(\frac{d C_{\text{atm}}}{dt}\right)_{C_{\text{in}}} = C_{\text{in}} \times 10^{15} / 12 \quad (17)$$

is added where C_{in} is in units of Pg C y^{-1} .

6 Sediments

The sediment model calculates $\%\text{CaCO}_3$ (dry weight) in the seafloor-bioturbated (mixed) sediment layer of thickness h_s as a function of sediment rain, dissolution, burial, and chemical erosion (for more details see Zeebe and Zachos, 2007). The model is particularly useful for long-term integrations and has been constructed similar to other models of this class (e.g. Keir, 1982; Sundquist, 1986; Sigman et al., 1998). However, the current model also includes variable porosity – a feature critical to simulating strong dissolution events that lead to sediment erosion, such as expected for the future or during the PETM (Zeebe and Zachos, 2007; Zeebe et al., 2008, 2009).

6.1 Chemical erosion

When dissolution of CaCO_3 exceeds the rain of CaCO_3 plus refractory material such as clay, the sediment column shrinks and previously deposited, underlying sediment

Title Page

Abstract

Introduction

Conclusions

References

Tables

Figures



Back

Close

Full Screen / Esc

Printer-friendly Version

Interactive Discussion



is reintroduced into the top layer and exposed to dissolution. This is referred to as chemical erosion. As a result, significantly more CaCO_3 is available for dissolution during erosion than originally contained in the top sediment layer. Once the top layer is entirely filled with clay, the sediment column is “sealed” and dissolution ceases. In order to fill the sediment top layer with clay, the sediment volume that was initially filled with CaCO_3 + pore water must be replaced by clay + pore water. Thus, if the sediment porosity ϕ is constant, the ratio of total CaCO_3 available during erosion to the mass contained in the original surface layer is given by:

$$1 + \frac{f^{\text{ci}}}{(1 - f^{\text{ci}})} \quad (18)$$

(Broecker and Takahashi, 1977) where f^{ci} and $(1 - f^{\text{ci}})$ are the initial CaCO_3 and clay dry weight fraction of the sediment, respectively. However, if porosity varies with % CaCO_3 (as observations show, see below), the ratio of total dissolved to initial CaCO_3 is given by:

$$1 + \frac{1 - \phi_0}{1 - \phi_1} \frac{f^{\text{ci}}}{1 - f^{\text{ci}}} \quad (19)$$

where ϕ_0 and ϕ_1 are the porosities of a pure clay and calcite layer, respectively. The factor $(1 - \phi_0)/(1 - \phi_1)$ is of the order 0.3–0.5 and therefore significant as it reduces the erodible CaCO_3 from below the bioturbated layer by 50–70 % compared to the constant ϕ estimate (Archer, 1996).

6.2 Variable porosity

In many locations, it has been observed that porosity decreases with greater CaCO_3 fraction f^{c} (e.g. Mayer, 1991; Herbert and Mayer, 1991; deMenocal et al., 1993). That is, sediment with high CaCO_3 content has a higher concentration of total solids per

Title Page

Abstract

Introduction

Conclusions

References

Tables

Figures



Back

Close

Full Screen / Esc

Printer-friendly Version

Interactive Discussion



unit volume than low carbonate sediment. The relationship between ϕ and f^c for a sediment layer composed of CaCO_3 , clay, and pore water is given by:

$$\phi = \frac{\phi_0 + f^c F_\phi}{1 + f^c F_\phi} \quad (20)$$

where $F_\phi = (\phi_1 - \phi_0)/(1 - \phi_1)$. The sediment model uses variable porosity as given by Eq. (20) and values for ϕ_0 and ϕ_1 as given in Table 3. Note that using the non-linear Eq. (20) in the model leads to the correct ratio of initial to erodible CaCO_3 (cf. Eq. 19, which was independently derived based on the geometry of the problem), while a linear relationship, for instance, would not.

6.3 Sediment model equations (single sediment box)

At every time step, calcite and clay rain of solid density ρ_s is added to the top sediment layer of thickness h_s (see Table 3 for values). Dissolution of calcite reduces the calcite content and net accumulation is hence rain minus dissolution. At the bottom of the sediment mixed layer, an amount equal to net accumulation is removed via burial. If dissolution of CaCO_3 exceeds the rain of CaCO_3 plus clay, chemical erosion occurs. The sediment model thus has to provide equations to calculate rain, dissolution, burial, and erosion. At variable porosity, the top layer can be separated into pure calcite plus pore water at porosity ϕ_1 (volume = $A h_1$) and pure clay plus pore water at porosity ϕ_0 (volume = $A h_2$). For variable porosity, the model equations can be conveniently written in terms of dh_1/dt . Conversion to df^c/dt merely requires multiplication by a factor (see below).

In case rain exceeds dissolution, no erosion needs to be considered and we can write for a single sediment box:

Title Page

Abstract

Introduction

Conclusions

References

Tables

Figures



Back

Close

Full Screen / Esc

Printer-friendly Version

Interactive Discussion



$$\frac{dh_1}{dt} = r^{cs} - r^d - w^c \quad (21)$$

where r^{cs} is the calcite rain rate, r^d is the calcite dissolution rate, and w^c is the calcite burial rate. All rates refer to volume of calcite plus pore water per unit area and time (unit m y^{-1}) at porosity ϕ_1 . Total rates of calcite + clay + pore water are denoted by r^s and w . Burial equals rain minus dissolution, i.e. $w = r^s - r^d$, and the condition for no erosion is $w > 0$. The rain rate of calcite, r^{cs} , depends on the carbon export, the rain ratio, and the fraction of water column dissolution. In the low latitudes, for instance, r^{cs} is given by:

$$r^{cs} = F_{\text{epl}} r_{\text{rain}}^{-1} (1 - v_{\text{wc}}) \times k^* \quad (22)$$

where F_{epl} is the low-latitude carbon export (in units of $\text{mol m}^{-2} \text{yr}^{-1}$), r_{rain} is the rain ratio ($\text{C}_{\text{org}} : \text{CaCO}_3$), v_{wc} is the CaCO_3 fraction dissolved in the water column (Table 2), $k^* = k^0 / [\rho_s (1 - \phi_1)]$ converts from $\text{mol m}^{-2} \text{yr}^{-1}$ to m y^{-1} , and $k^0 = (100/10^3) \text{kg mol}^{-1}$ converts from mol CaCO_3 to kg CaCO_3 . The rain rate of refractory material, r^{rs} , is calculated correspondingly based on F_{rrf} (Table 3) and the total rain r^s is given by

$r^s = r^{cs} + r^{rs}$.
The dissolution rate, r^d , is calculated as:

$$r^d = R^d \times k^* \quad (23)$$

where R^d is given by the following expression at modern seawater Mg/Ca ratio (Sigman et al., 1998):

$$R^d = (f^c)^{0.5} K_{sd} ([\text{CO}_3^{2-}]_{\text{sat}} - [\text{CO}_3^{2-}])^{n_{sd}} (c^0)^{-n_{sd}} \quad \text{if } [\text{CO}_3^{2-}] < [\text{CO}_3^{2-}]_{\text{sat}} \quad (24)$$

$$R^d = 0 \quad \text{otherwise} \quad (25)$$

where K_{sd} and n_{sd} are “effective” rate parameters (see below), $[\text{CO}_3^{2-}]_{\text{sat}}$ and $[\text{CO}_3^{2-}]$ is the carbonate ion concentration at calcite saturation and in the bottom water, respectively, and $c^0 = 1 \text{ mol kg}^{-1}$ so that R^d is in units of $\text{mol m}^{-2} \text{yr}^{-1}$. It is important to note

Title Page

Abstract

Introduction

Conclusions

References

Tables

Figures

◀

▶

◀

▶

Back

Close

Full Screen / Esc

Printer-friendly Version

Interactive Discussion



that the effective rate parameters K_{sd} and n_{sd} relate *bottom* water undersaturation to dissolution rate (Keir, 1982; Sundquist, 1986; Sigman et al., 1998; Zeebe and Zachos, 2007, see Table 3 for values). They are not be confused with reaction parameters relating *porewater* undersaturation to dissolution rate such as the calcite reaction order n (typically $n = 4.5$).

Finally, an expression is needed for the calcite burial, w^c , as a function of total burial w . The thickness of the pure calcite layer within $\Delta z (= w \Delta t)$ can be expressed as $f^c \Delta z (1 - \phi)$ but also as $1 \cdot \Delta h_1 (1 - \phi_1)$ (calcite fraction = 1), which gives:

$$\Delta h_1 = f^c \Delta z \frac{1 - \phi}{1 - \phi_1} \quad (26)$$

or expressed per unit time as a rate:

$$w^c = f^c w \frac{1 - \phi}{1 - \phi_1} \quad (27)$$

As a result, all rates have now been expressed by model-predicted quantities and thus by inserting Eqs. (22), (23), and (27) into (21), the change in calcite content per time step can be computed. Because we took care of all individual porosities, the relationship between ϕ and f^c , Eq. (20), is obeyed automatically.

In case of erosion ($w < 0$), it can be shown that:

$$\frac{dh_1}{dt} = -(1 - f^{ci}) (-w) \frac{1 - \phi^i}{1 - \phi_0} - r^{rs} \quad (28)$$

where f^{ci} and ϕ^i is the initial calcite fraction and porosity, respectively, and r^{rs} is the clay rain rate (see above). The total dissolution of pure calcite can be derived as:

$$\frac{dh^{dc}}{dt} = [(-w) + r^{rs}] (1 - \phi_1) \quad (29)$$

In other words, all calcite in Δz and calcite rain is dissolved. In addition, calcite is being replaced by the clay in Δz and by the clay rain (equivalent calcite is also dissolved).

Title Page

Abstract

Introduction

Conclusions

References

Tables

Figures



Back

Close

Full Screen / Esc

Printer-friendly Version

Interactive Discussion



Finally, the sediment model can also be formulated in terms of f^c by simply multiplying by a factor:

$$\frac{df^c}{dt} = \frac{dh_1}{dt} G^{-1} = (r^{cs} - r^d - w^c) G^{-1}, \quad (30)$$

where

$$G = \frac{h_s}{1 - \phi_1} \left[(1 - \phi) - f^c \frac{\partial \phi}{\partial f^c} \right] \quad (31)$$

and

$$\frac{\partial \phi}{\partial f^c} = \frac{F_\phi (1 - \phi_0)}{(1 + f^c F_\phi)^2} \quad (32)$$

with $F_\phi = (\phi_1 - \phi_0)/(1 - \phi_1)$.

6.4 Sediment model equations (all sediment boxes)

Let y_n be a subset of \mathbf{y} (Eq. 1), representing the CaCO_3 dry fraction (f^c) in sediment boxes at different depth levels in the different ocean basins. If the total number of depth levels is NSD and the total number of ocean basins is NOC (Table 1), then the total number of equations for all sediment boxes is NSD \times NOC. Based on Eq. (30), the differential equation for the CaCO_3 dry fraction in sediment box j is:

$$\frac{dy_n}{dt} = \frac{d(f_j^c)}{dt} = (r_j^{cs} - r_j^d - w_j^c) G_j^{-1} \quad (33)$$

where $j = 1, 2, \dots, \text{NSD}$ for the first ocean basin (Atlantic), $j = \text{NSD} + 1, \text{NSD} + 2, \dots, 2\text{NSD}$ for the second ocean basin (Indian), and so on. In case of dissolution, TCO_2 and TA are returned to the ocean, giving rise to the sediment source term in the ocean tracer equation (cf. Eq. 2):

$$V_k \left(\frac{d[\text{TCO}_2]_k}{dt} \right)_{\text{sed}} = \sum A_j^{\text{sed}} R_j^{\text{d}} \quad (34)$$

$$V_k \left(\frac{d[\text{TA}]_k}{dt} \right)_{\text{sed}} = 2 \sum A_j^{\text{sed}} R_j^{\text{d}} \quad (35)$$

where each sum runs over all sediment boxes j located within the area and depth range of ocean box k . The surface area of sediment box j is denoted by A_j^{sed} .

7 Miscellaneous

7.1 Ocean carbonate chemistry

Carbonate chemistry parameters for modern seawater composition are calculated based on equilibrium constants on the total $p\text{H}$ scale (Lueker et al., 2000; Zeebe and Wolf-Gladrow, 2001). The C program uses a simplified and fast numerical routine to compute CO_2 parameters from TCO_2 and TA (Follows et al., 2006). If applied properly, the method yields accurate results that are essentially identical to those obtained with standard routines (Zeebe and Wolf-Gladrow, 2001). The method was originally devised to compute modern carbonate chemistry parameters in biogeochemical models where conditions change little between consecutive time steps (Follows et al., 2006). This is not necessarily always the case in LOSCAR and can lead to failure in rare cases. For instance, if the model is initiated with a very high TA/ TCO_2 ratio, the calculated H^+ concentration may become negative. The user is warned in such instances and is advised to change the initial conditions. Again, such cases are probably rare. In fairness, it should also be noted that non-standard chemistry conditions (which can occur in LOSCAR), are beyond the original intend of the method (Follows et al., 2006). Apart from the limitation mentioned above, the method is easy to implement, sufficiently accurate, and computationally efficient.

Title Page

Abstract

Introduction

Conclusions

References

Tables

Figures

◀

▶

◀

▶

Back

Close

Full Screen / Esc

Printer-friendly Version

Interactive Discussion



7.2 Paleocene/Eocene ocean chemistry

Paleocene/Eocene seawater conditions were different from modern conditions owing to factors such as temperature and major ion composition of seawater, including the seawater Mg/Ca ratio (e.g Tyrrell and Zeebe, 2004). These factors can significantly affect thermodynamic quantities such as equilibrium constants and solubility products, which in turn have a major impact on the predicted ocean carbonate chemistry and atmospheric CO₂. The chemistry routines implemented in LOSCAR allow for variations in, for instance, temperature, salinity, and the concentrations of Mg²⁺ and Ca²⁺ in seawater. For example, due to warmer surface and bottom water temperatures in the late Paleocene and Eocene, the calcite saturation concentration at a bottom water temperature of 14–17 °C during the PETM is quite different from the modern at 2 °C (see Fig. 3 of Zeebe and Zachos, 2007). This effect is included in LOSCAR by using temperature-dependent equations for the solubility product of carbonate minerals (Mucci, 1983). Pressure corrections for solubility products and equilibrium constants are based on Millero (1995) and references therein; for the latest revisions, check: www.soest.hawaii.edu/oceanography/faculty/zeebe_files/CO2_System_in_Seawater/csyst.html.

Furthermore, the P/E-simulations use [Mg²⁺] = 30 mmol kg⁻¹ and [Ca²⁺] = 20 mmol kg⁻¹ rather than the modern values of [Mg²⁺] = 53 mmol kg⁻¹ and [Ca²⁺] = 10 mmol kg⁻¹ (Tyrrell and Zeebe, 2004; Zeebe et al., 2009). The effect of seawater Mg²⁺ and Ca²⁺ on the first and second dissociation constant of carbonic acid is estimated using sensitivity coefficients (Ben-Yaakov and Goldhaber, 1973):

$$s_{K^*} = \frac{\Delta K^*/K^*}{\Delta c_i/c_i} \quad (36)$$

where ΔK^* is the change in K^* due to the relative change in concentration, $\Delta c_i/c_i$, of component i . Using $\Delta c/c = (c - c_m)/c_m$, where $m = \text{modern}$, it follows:

GMDD

4, 1435–1476, 2011

LOSCAR

R. E. Zeebe

Title Page

Abstract

Introduction

Conclusions

References

Tables

Figures

◀

▶

◀

▶

Back

Close

Full Screen / Esc

Printer-friendly Version

Interactive Discussion



$$\Delta K^* = s_{K^*} K^* (c/c_m - 1) \quad (37)$$

and finally:

$$K^* = K_m^* + \Delta K_{Mg^{2+}}^* + \Delta K_{Ca^{2+}}^* \quad (38)$$

Sensitivity parameters for the effect of Mg^{2+} and Ca^{2+} on K^* are (Ben-Yaakov and Goldhaber, 1973):

$$s_{K_1^*} = 155 \times 10^{-3} ; \quad s_{K_2^*} = 442 \times 10^{-3} \quad \text{for } Mg^{2+} \quad (39)$$

$$s_{K_1^*} = 33.73 \times 10^{-3} ; \quad s_{K_2^*} = 38.85 \times 10^{-3} \quad \text{for } Ca^{2+} \quad (40)$$

With these sensitivity parameters, and the modern and paleo-concentrations of Mg^{2+} and Ca^{2+} (see above), the correction to equilibrium constants (Eq. 38) can be applied.

Seawater Mg^{2+} and Ca^{2+} also affect the calcite solubility product, K_{sp}^* , and thus the steady-state deep-sea $[CO_3^{2-}]$. Following Mucci and Morse (1984), the stoichiometric solubility product drops with decreasing seawater Mg/Ca ratio. In other words, Eocene K_{sp}^* would have been smaller and, given roughly constant deep-sea saturation state, $[CO_3^{2-}]$ would also have been smaller than modern. The data of Mucci and Morse (1984) may be fitted to an equation of the form:

$$K_{sp}^* = K_{sp,m}^* [1 - \alpha (x_m - x)] \quad (41)$$

where m = modern, $\alpha = 0.0833$, and $x = Mg/Ca$. Using modern and P/E-values for $[Mg^{2+}]$ and $[Ca^{2+}]$ as given above, the stoichiometric solubility product of calcite would have been reduced by about 30 %, compared to modern.

Another important consequence of changes in oceanic Ca^{2+} , for instance, is its effect on the ocean carbon inventory. The long-term carbon inventory and carbonate chemistry of the ocean-atmosphere system is controlled by atmospheric CO_2 and the

Title Page

Abstract

Introduction

Conclusions

References

Tables

Figures



Back

Close

Full Screen / Esc

Printer-friendly Version

Interactive Discussion



balance between riverine flux and carbonate burial (Zeebe and Caldeira, 2008). Carbonate burial is tied to the deep-sea carbonate saturation, which is proportional to the product of $[Ca^{2+}] \times [CO_3^{2-}]$. If oceanic $[Ca^{2+}]$ doubles at constant saturation state, $[CO_3^{2-}]$ would drop by 50% (even more if the effect of Mg/Ca on K_{sp}^* is accounted for). For example, $[CO_3^{2-}]$ prior to the PETM was hence much lower than modern Paleocene/Eocene $[Ca^{2+}]$ was 20 mmol kg⁻¹. In the model, this leads to a pre-PETM ocean carbon inventory that is similar to the modern value, despite a higher baseline atmospheric CO₂ at the time.

7.3 Temperature sensitivity

The initial temperature of each individual ocean box is set at the start of the run. Throughout the run, temperature can be held constant, be manipulated based on user input, or be computed based on a simple expression for the sensitivity of temperature to changes in atmospheric CO₂ as calculated by the model (cf. Archer, 2005). In order to provide a flexible and numerically stable option, the C version of the program includes temperature as an ocean tracer variable. The temperature of ocean box k ($T_{C,k}$ in °C) is assumed to respond to a change in pCO_2 with a certain time lag and relax towards equilibrium temperature. The equilibrium temperature of box k is given by:

$$T_{C,k}^{eq} = T_{C,k}^0 + s \ln(pCO_2/pCO_2^0) / \ln(2), \quad (42)$$

where the superscript “0” refers to the initial (steady-state) temperature and pCO_2 , respectively, and s is the prescribed temperature increase per doubling of atmospheric CO₂. The parameter s as used here is conceptually similar to what is generally referred to as “climate sensitivity”. However, the precise meaning of s will have to be defined properly for each specific application in the context of the time scales and feedbacks involved (see Zeebe, 2011).

[Title Page](#)
[Abstract](#)
[Introduction](#)
[Conclusions](#)
[References](#)
[Tables](#)
[Figures](#)
[Back](#)
[Close](#)
[Full Screen / Esc](#)
[Printer-friendly Version](#)
[Interactive Discussion](#)


The differential equation for the temperature of ocean box k then reads:

$$\frac{d(T_{C,k})}{dt} = (T_{C,k}^{\text{eq}} - T_{C,k}) / \tau_n \quad (43)$$

where τ_n is the relaxation time, which can take on three different values depending on whether k refers to a surface, intermediate, or deep box (Table 2).

7.4 Numerics

As mentioned above, the equations solved in LOSCAR are typically stiff and require an appropriate solver for the problem. The LOSCAR C-version uses a fourth-order Rosenbrock method with automatic stepsize adjustment (Press et al., 1992). For these kind of solvers, it is critical to scale the variables properly. Thus, variables have been scaled to order 1, if necessary, by multiplying by arbitrary factors before passing to the solver. This includes, for instance, atmospheric carbon and temperature (see Sects. 5 and 7.3).

The carbonate dissolution flux, R^d is proportional to the square root of the CaCO_3 fraction f^c (Eq. 24). It turned out that during strong dissolution, f^c occasionally became negative when the CaCO_3 fraction approached zero. This issue has been eliminated (in most cases) by using a linear relationship between f^c and R^d when f^c drops below a certain threshold value f_{sm}^c . The threshold value can be changed by the user and should be increased if f^c still becomes negative during a run. Another option is to increase the solver accuracy by reducing the value of ε_{siv} (the default value is usually not very accurate).

LOSCAR is quick. Running the fossil fuel scenario over 1250 yr (Fig. 5) using the LOSCAR C code compiled under Linux with gcc 4.4.3, without optimization and default ε_{siv} , takes less than 2 s wall clock time on a current standard desktop machine with Intel Core2 Duo E8500 @3.16GHz (no other CPU-demanding processes running). The computational efficiency makes LOSCAR an ideal tool for multi-parameter variations that require a large number of model runs (e.g. Zeebe et al., 2008, 2009).

Title Page

Abstract

Introduction

Conclusions

References

Tables

Figures

◀

▶

◀

▶

Back

Close

Full Screen / Esc

Printer-friendly Version

Interactive Discussion



8 Tuning

In order for LOSCAR to provide model output that resembles observations, several model parameters require tuning. This includes mixing coefficients, biological export fluxes, remineralization fraction (intermediate vs. deep box), rain ratio, and water column dissolution (see Table 2). The tuning is based on comparison between model-predicted variables and modern observations. For example, parameters were tuned by requiring the ocean tracer variables TCO_2 and TA in the various model boxes to match GLODAP data, averaged over the area and depth range of the corresponding boxes (Key et al., 2004). Note that TCO_2 data were corrected for anthropogenic carbon by subtracting 45 and 25 $\mu\text{mol kg}^{-1}$ from the surface and intermediate values, respectively (see below for $\delta^{13}\text{C}$ -corrections). The agreement between model and data is satisfactory (see Fig. 4). As a result, the global preindustrial TCO_2 inventory in LOSCAR is 35 920 PgC vs. 35 760 PgC based on GLODAP data (Key et al., 2004). Similarly, model PO_4 and oxygen were compared to data summarized in the World Ocean Atlas (WOA05, 2005). Again, the agreement between model and data is adequate, except perhaps for the oxygen content in intermediate boxes, which appears to be underestimated by the model. This could be improved. However, it would come at the expense of a larger mismatch in the deep boxes. This was avoided because for our LOSCAR applications so far, the properties of the deep boxes were more important than those of the intermediate boxes.

Another variable used for parameter tuning is the stable carbon isotope composition of TCO_2 ($\delta^{13}\text{C}_{\text{TCO}_2}$), which was matched to the data of Kroopnick (1985). Note that due to the ocean's uptake of fossil fuel carbon (which is isotopically light, i.e. depleted in ^{13}C), the ocean's $\delta^{13}\text{C}_{\text{TCO}_2}$ is continuously dropping (so-called Suess effect). Thus, for preindustrial tuning, the early $\delta^{13}\text{C}$ -data sets are more useful than the most recent ones, which are increasingly contaminated with anthropogenic carbon. Nevertheless, Kroopnick (1985) estimated that surface ocean $\delta^{13}\text{C}_{\text{TCO}_2}$ had already dropped by $\sim 0.5\text{‰}$ and that the average $\delta^{13}\text{C}_{\text{TCO}_2}$ of the preindustrial surface ocean was about

Title Page

Abstract

Introduction

Conclusions

References

Tables

Figures



Back

Close

Full Screen / Esc

Printer-friendly Version

Interactive Discussion



2.5‰. This surface value was used for model parameter tuning (Fig. 4). As a result, the preindustrial $\delta^{13}\text{C}$ of atmospheric CO_2 is -6.38‰ in LOSCAR vs. -6.30 to -6.40‰ based on ice core and firn data (e.g. Francey et al., 1999).

Adequate model values for the steady-state carbonate ion concentration in the deep boxes are important for both the ocean and the sediment model component. After parameter tuning, the preindustrial deep-sea $[\text{CO}_3^{2-}]$ as predicted by LOSCAR and calculated based on GLODAP data (Key et al., 2004) are in good agreement (Fig. 4). The preindustrial inventory of CaCO_3 in the seafloor-bioturbated sediment layer (in units of carbon) is about 800 Pg C, close to the value of more complex models (e.g. Archer et al., 1998).

In summary, after model-data comparison including all variables shown in Fig. 4, the values for the parameters labeled “tuned” in Table 2 were obtained. The preindustrial (steady-state) $p\text{CO}_2$ in the model was set to 280 ppmv by assigning this value to $p\text{CO}_2^0$, which drives the system towards the desired steady-state $p\text{CO}_2$ via the silicate weathering equation (Eq. 12). Regarding the Paleocene/Eocene model setup, several key parameters such as deep-sea $[\text{CO}_3^{2-}]$ and the calcite compensation depth (CCD) before and during the PETM have been discussed elsewhere and are not repeated here (see Zeebe et al., 2009, Supplementary Information). The pre-PETM inventory of CaCO_3 in the seafloor-bioturbated sediment layer (in units of carbon) is about 620 Pg C. The initial (steady-state) partial pressure of atmospheric CO_2 was set to 1000 ppmv in our P/E-simulations. Although this value falls within the (large) range of available proxy estimates, it is somewhat arbitrary. The user is welcome to change the initial $p\text{CO}_2$ value in the P/E-setup.

Title Page

Abstract

Introduction

Conclusions

References

Tables

Figures



Back

Close

Full Screen / Esc

Printer-friendly Version

Interactive Discussion



9 Input/output examples

9.1 Fossil fuel emission scenario

LOSCAR can read in files that supply a time series of fossil fuel emissions in order to project future changes in atmospheric CO₂, surface ocean pH, calcite and aragonite saturation, and other variables (cf. Zeebe et al., 2008, Supporting Online Material). For example, Fig. 5 shows results obtained with LOSCAR for a fossil fuel emission scenario with a total carbon release of 1000 Pg C over 500 yr. Note that the results differ slightly from those in Zeebe et al. (2008) because ocean temperature was held constant here for simplicity. The initial conditions from which the scenario was started are the pre-industrial steady-state conditions shown in Fig. 4. No changes in the biological pump were assumed (PO₄ is constant). The temperature of the low- and high-latitude box is 20 and 2 °C, respectively (Table 2). This temperature difference is mostly responsible for the difference in carbonate ion concentration ([CO₃²⁻]) and saturation state (Ω) between low- and high-latitude surface boxes. Note that while TCO₂ in the surface boxes responds immediately to the fossil fuel carbon release, there is a delay in TA, which only starts rising once sediment dissolution commences and the calcite compensation depth (CCD) starts shallowing (cf. Ilyina et al., 2009).

9.2 Paleocene-Eocene Thermal Maximum

Using appropriate boundary conditions, LOSCAR can also be used to simulate time intervals or events of the past such as the PETM. During the PETM, a large mass of carbon was released into Earth's surface reservoirs (e.g. Dickens et al., 1995; Zachos et al., 2005; Dickens, 2011), while surface temperatures rose by 5–9 °C within a few thousand years. Figure 6 shows results for a PETM scenario with an initial carbon input of 3000 Pg C over a few thousand years, which yielded close agreement with observations (for more details, see Zeebe et al., 2009). Note that the time interval of the integration now covers 200 ky ($t = 0$ refers to the P/E boundary), rather than a few

Title Page

Abstract

Introduction

Conclusions

References

Tables

Figures



Back

Close

Full Screen / Esc

Printer-friendly Version

Interactive Discussion



millennia as in the previous example. Changes in boundary conditions compared to the modern setup include a Paleocene/Eocene bathymetry (Bice and Marotzke, 2002), addition of the Tethys ocean, different seawater chemistry (see Sect. 7.2), and different circulation patterns (see Fig. 2). Furthermore, the PETM simulations use different initial conditions for e.g. temperature, steady-state $p\text{CO}_2^0$, weathering fluxes etc. (Tables 2 and 3).

At steady-state $p\text{CO}_2^0$ of 1000 ppmv, but similar carbonate mineral saturation state as in the modern ocean, the steady-state pH of the Paleocene/Eocene ocean would have been lower than modern (Fig. 6). Because of higher seawater Ca^{2+} and the effect of Mg/Ca on the solubility product of calcite, the initial carbonate ion concentration in the P/E-simulations is substantially lower than in the modern ocean (cf. Sect. 7.2). As a result, steady-state TCO_2 and TA are similar to modern values despite higher $p\text{CO}_2$ (Fig. 6). Note that the Atlantic CCD shoals dramatically during the event, while there is little response in the Pacific CCD, consistent with observations (Zachos et al., 2005; Zeebe et al., 2009; Leon-Rodriguez and Dickens, 2010). The “overshoot” of the CCD, i.e. the fact that its position is deeper at $t > 80$ ky than its initial position, is a direct consequence of the weathering feedback (see Sect. 4) and is also in agreement with observations (e.g. Kelly et al., 2005). At $t > 80$ ky, atmospheric $p\text{CO}_2$ is still elevated over the initial $p\text{CO}_2^0$ (Fig. 6), which causes enhanced weathering of carbonates and silicates. The enhanced weathering raises the ocean’s saturation state and deepens the CCD until a quasi steady-state of riverine flux and burial has been established. The quasi steady-state ($t > 80$ ky) must be maintained at a CCD deeper than the initial depth (because of enhanced burial) until atmospheric $p\text{CO}_2$ and weathering fluxes have returned to their initial steady-state values. This explains the “overshoot” of the CCD.

[Title Page](#)[Abstract](#)[Introduction](#)[Conclusions](#)[References](#)[Tables](#)[Figures](#)[Back](#)[Close](#)[Full Screen / Esc](#)[Printer-friendly Version](#)[Interactive Discussion](#)

10 Summary

LOSCAR is a useful tool to tackle carbon cycle problems on various time scales as demonstrated in earlier applications that dealt with future projections of ocean chemistry and weathering, $p\text{CO}_2$ sensitivity to carbon cycle perturbations throughout the Cenozoic, and carbon/calcium cycling during the PETM (Zeebe et al., 2008, 2009; Uchikawa and Zeebe, 2008; Stuecker and Zeebe, 2010; Uchikawa and Zeebe, 2010; Komar and Zeebe, 2011; Zeebe and Ridgwell, 2011). The present contribution has provided a coherent description of the LOSCAR model. The description will hopefully be beneficial to the readership of the journal, as well as users of the model. I anticipate that future applications will reveal the full spectrum of problems suitable to be studied with LOSCAR. The LOSCAR source code in C can be obtained from the author by sending a request to loscar.model@gmail.com.

References

- Archer, D. E.: An atlas of the distribution of calcium carbonate in sediments of the deep sea, *Global Biogeochem. Cy.*, 10(1), 159–174, 10.1029/95GB03016, 1996. 1447
- Archer, D. E.: Fate of fossil fuel CO_2 in geologic time, *J. Geophys. Res.*, 110(1012), C09S05, doi:10.1029/2004JC002625, 2005. 1455
- Archer, D. E., Kheshgi, H., and Maier-Reimer, E.: Dynamics of fossil fuel CO_2 neutralization by marine CaCO_3 , *Global Biogeochem. Cy.*, 12, 259–276, 1998. 1442, 1458
- Ben-Yaakov, S. and Goldhaber, M. B.: The influence of sea water composition on the apparent constants of the carbonate system, *Deep-Sea Res.*, 20, 87–99, 1973. 1453, 1454
- Berner, R. A., Lasaga, A. C., and Garrels, R. M.: The carbonate-silicate geochemical cycle and its effect on atmospheric carbon dioxide over the past 100 million years, *Am. J. Sci.*, 283, 641–683, 1983. 1444
- Bice, K. L. and Marotzke, J.: Could changing ocean circulation have destabilized methane hydrate at the Paleocene/Eocene boundary?, *Paleoceanogr.*, 17, 1018, doi:10.1029/2001PA00678, 2002. 1439, 1460, 1467, 1472

GMDD

4, 1435–1476, 2011

LOSCAR

R. E. Zeebe

Title Page

Abstract

Introduction

Conclusions

References

Tables

Figures



Back

Close

Full Screen / Esc

Printer-friendly Version

Interactive Discussion



[Title Page](#)[Abstract](#)[Introduction](#)[Conclusions](#)[References](#)[Tables](#)[Figures](#)[Back](#)[Close](#)[Full Screen / Esc](#)[Printer-friendly Version](#)[Interactive Discussion](#)

- Broecker, W. S. and Peng, T.-H.: The role of CaCO_3 compensation in the glacial to interglacial atmospheric CO_2 change, *Global Biogeochem. Cy.*, 1, 15–29, 1987. 1443
- Broecker, W. S. and Peng, T.-H.: *Greenhouse Puzzles: Keelings's World, Martin's World, Walker's World*, 2nd Edn., Eldigio Press, Palisades, New York, 1998. 1468
- 5 Broecker, W. S. and Takahashi, T.: Neutralization of fossil fuel CO_2 by marine calcium carbonate, in: *The Fate of Fossil Fuel CO_2 in the Oceans*, edited by: Anderson, N. R. and A. Malahoff, 213–241, Plenum Press, New York, 1977. 1447
- deMenocal, P. B., Ruddiman, W. F., and Pokras, E. M.: Influences of high- and low-latitude processes on African climate: Pleistocene eolian records from equatorial Atlantic Ocean Drilling Program Site 663, *Paleoceanogr.*, 8(2), 209–242, 1993. 1447
- 10 Dickens, G. R.: Methane release from gas hydrate systems during the Paleocene-Eocene thermal maximum and other past hyperthermal events: setting appropriate parameters for discussion, *Clim. Past Discuss.*, 7, 1139–1174, doi:10.5194/cpd-7-1139-2011, 2011. 1459
- Dickens, G. R., O'Neil, J. R., Rea, D. K., and Owen, R. M.: Dissociation of oceanic methane hydrate as a cause of the carbon isotope excursion at the end of the Paleocene, *Paleoceanogr.*, 10, 965–971, 1995. 1459
- 15 Feely, R. A., Sabine, C. L., Lee, K., Millero, F. J., Lamb, M. F., Greeley, D., Bullister, J. L., Key, R. M., Peng, T.-H., Kozyr, A., Ono, T., and Wong, C. S.: In situ calcium carbonate dissolution in the Pacific Ocean, *Global Biogeochem. Cyc.*, 16(4), 1144, doi:10.1029/2002GB001866, 2002. 1442
- 20 Follows, M. J., Ito, T., and Dutkiewicz, S.: On the solution of the carbonate chemistry system in ocean biogeochemistry models, *Ocean Model.*, 12, 290–301, doi:10.1016/j.ocemod.2005.05.004, 2006. 1452
- Francey, R. J., Allison, C. E., Etheridge, D. M., Trudinger, C. M., Enting, I. G., Leuenberger, M., Langenfelds, R. L., Michel, E., and Steele, L. P.: A 1000-year high precision record of $\delta^{13}\text{C}$ in atmospheric CO_2 , *Tellus*, 51B, 170–193, 1999. 1458
- 25 Herbert, T. D. and Mayer, L. A.: Long climatic time series from sediment physical property measurements, *J. Sed. Petrol.*, 61(7), 1089–1108, 1991. 1447
- Ilyina, T., Zeebe, R. E., Maier-Reimer, E., and Heinze, C.: Early detection of ocean acidification effects on marine calcification, *Global Biogeochem. Cy.*, 23, GB1008, doi:10.1029/2008GB003278, 2009. 1459
- 30 Keir, R.: Dissolution of calcite in the deep sea: Theoretical predictions for the case of uniform size particles settling into a well-mixed sediment, *Am. J. Sci.*, 282, 193–236, 1982. 1446,

1450, 1469

Kelly, D. C., Zachos, J. C., Bralower, T. J., and Schellenberg, S. A.: Enhanced terrestrial weathering/runoff and surface-ocean carbonate production during the recovery stages of the Paleocene-Eocene Thermal Maximum, *Paleoceanogr.*, 20, PA4023, doi:10.1029/2005PA001163, 2005. 1460

Key, R. M., Kozyr, A., Sabine, C. L., Lee, K., Wanninkhof, R., Bullister, J., Feely, R. A., Millero, F., Mordy, C., and Peng, T.-H.: A global ocean carbon climatology: Results from GLODAP, *Global Biogeochem. Cy.*, 18, GB4031, doi:10.1029/2004GB002247, 2004. 1457, 1458

Köhler, P., Fischer, H., and Zeebe, R. E.: Quantitative interpretation of atmospheric carbon records over the last glacial termination, *Global Biogeochem. Cy.*, 19, GB4020, doi:10.1029/2004GB002345, 2005. 1436

Komar, N. and Zeebe, R. E.: Changes in oceanic calcium from enhanced weathering did not affect calcium-based proxies during the Paleocene-Eocene Thermal Maximum, *Paleoceanography*, 26, doi:10.1029/2010PA001979, in press, 2011. 1437, 1461

Kroopnick, P. M.: The distribution of ^{13}C of ΣCO_2 in the world oceans, *Deep-Sea Res. I*, 32, 57–84, 1985. 1457

Leon-Rodriguez, L. and Dickens, G. R.: Constraints on ocean acidification associated with rapid and massive carbon injections: The early Paleogene record at ocean drilling program site 1215, equatorial Pacific Ocean, *Palaeogeogr. Palaeoclimatol. Palaeoecol.*, 298, 409–420, 2010. 1460

Lueker, T. J., Dickson, A. G., and Keeling, C. D.: Ocean $p\text{CO}_2$ calculated from dissolved inorganic carbon, alkalinity, and equations for K_1 and K_2 : validation based on laboratory measurements of CO_2 in gas and seawater at equilibrium, *Mar. Chem.*, 70, 105–119, 2000. 1452

Lunt, D. J., Valdes, P. J., Dunkley-Jones, T., Ridgwell, A., Haywood, A. M., Schmidt, D. N., Marsh, R., and Maslin, M.: CO_2 -driven ocean circulation changes as an amplifier of Paleocene-Eocene Thermal Maximum hydrate destabilization, *Geology*, 38, 875–878, doi:10.1130/G31184.1, 2010. 1472

Mayer, L. A.: Extraction of high-resolution carbonate data for palaeoclimate reconstruction, *Nature*, 352, 148–150, 1991. 1447

Menard, H. W. and Smith, S. M.: Hypsometry of Ocean Basin Provinces, *J. Geophys. Res.*, 71(18), 4305–4325, 1966. 1439

Millero, F. J.: Thermodynamics of the carbon dioxide system in the oceans, *Geochim. Cosmochim. Acta*, 59, 661–677, 1995. 1453

GMDD

4, 1435–1476, 2011

LOSCAR

R. E. Zeebe

Title Page

Abstract

Introduction

Conclusions

References

Tables

Figures

◀

▶

◀

▶

Back

Close

Full Screen / Esc

Printer-friendly Version

Interactive Discussion



[Title Page](#)[Abstract](#)[Introduction](#)[Conclusions](#)[References](#)[Tables](#)[Figures](#)[◀](#)[▶](#)[◀](#)[▶](#)[Back](#)[Close](#)[Full Screen / Esc](#)[Printer-friendly Version](#)[Interactive Discussion](#)

- Milliman, J. D., Troy, P. J., Balch, W. M., Adams, A. K., Li, Y.-H., and Mackenzie, F. T.: Biologically mediated dissolution of calcium carbonate above the chemical lysocline?, *Deep-Sea Res. I*, 46, 1653–1669, 1999. 1442
- Morse, J. W. and Mackenzie, F. T.: *Geochemistry of Sedimentary Carbonates*, Developments in sedimentology, 48, Elsevier, Amsterdam, 1990. 1469
- Mucci, A.: The solubility of calcite and aragonite in seawater at various salinities, temperatures, and one atmosphere total pressure, *Am. J. Sci.*, 283, 780–799, 1983. 1453
- Mucci, A. and Morse, J. W.: The solubility of calcite in seawater solutions of various magnesium concentration, $I_t = 0.697$ m at 25°C and one atmosphere total pressure, *Geochim. Cosmochim. Acta*, 48, 815–822, doi:10.1016/0016-7037(84)90103-0, 1984. 1454
- Munhoven, G. and Francois, L. M.: Glacial-interglacial variability of atmospheric CO₂ due to changing continental silicate rock weathering: A model study, *J. Geophys. Res.*, 101(D16), 21423–21437, 1996. 1436
- Press, W. H., Flannery, B. P., Teukolsky, S. A., and Vetterling, W. T.: *Numerical Recipes in C: The Art of Scientific Computing*, Cambridge University, Cambridge, 1020 pp., 1992. 1438, 1456
- Ridgwell, A. J.: *Glacial-interglacial perturbations in the global carbon cycle*, Ph.D. thesis, Univ. of East Anglia at Norwich, UK, 2001. 1436
- Sarmiento, J. L. and Toggweiler, J. R.: A new mode of the role of the oceans in determining atmospheric P_{CO_2} , *Nature*, 308, 621–624, 1984. 1436
- Shaffer, G., Malskær Olsen, S., and Pepke Pedersen, J. O.: Presentation, calibration and validation of the low-order, DCESS Earth System Model (Version 1), *Geosci. Model Dev.*, 1, 17–51, doi:10.5194/gmd-1-17-2008, 2008. 1437
- Sigman, D. M., McCorkle, D. C., and Martin, W. R.: The calcite lysocline as a constraint on glacial/interglacial low-latitude production changes, *Global Biogeochem. Cy.*, 12(3), 409–427, 1998. 1436, 1446, 1449, 1450, 1469
- Stuecker, M. F. and Zeebe, R. E.: Ocean chemistry and atmospheric CO₂ sensitivity to carbon perturbations throughout the Cenozoic, *Geophys. Res. Lett.*, 37, L03609, doi:10.1029/2009GL041436, 2010. 1437, 1461
- Sundquist, E. T.: *Geologic Analogs: Their value and limitations in carbon dioxide research*, in: *The Changing Carbon cycle: A Global Analysis*, edited by: Trabalka, J. R. and Reichle, D. E., 371–402 pp., Springer-Verlag, New York, 1986. 1436, 1446, 1450, 1469
- Thomas, D. J., Bralower, T. J., and Jones, C. E.: Neodymium isotopic reconstruction of late

[Title Page](#)[Abstract](#)[Introduction](#)[Conclusions](#)[References](#)[Tables](#)[Figures](#)[Back](#)[Close](#)[Full Screen / Esc](#)[Printer-friendly Version](#)[Interactive Discussion](#)

Paleocene-early Eocene thermohaline circulation, *Earth Planet Sci. Lett.*, 209, 309–322, 2003. 1472

Toggweiler, J. R.: Variation of atmospheric CO₂ by ventilation of the ocean's deepest water, *Paleoceanography*, 14(5), 571–588, 1999. 1436, 1439, 1467, 1468, 1472

5 Tyrrell, T. and Zeebe, R. E.: History of carbonate ion concentration over the last 100 million years, *Geochim. Cosmochim. Acta*, 68(17), 3521–3530, 2004. 1453

Uchikawa, J. and Zeebe, R. E.: Influence of terrestrial weathering on ocean acidification and the next glacial inception, *Geophys. Res. Lett.*, 35, L23608, doi:10.1029/2008GL035963, 2008. 1437, 1445, 1461, 1469

10 Uchikawa, J. and Zeebe, R. E.: Examining possible effects of seawater pH decline on foraminiferal stable isotopes during the Paleocene-Eocene Thermal Maximum, *Paleoceanography*, 25, PA2216, doi:10.1029/2009PA001864, 2010. 1437, 1461

Walker, J. C. G. and Kasting, J. F.: Effects of fuel and forest conservation on future levels of atmospheric carbon dioxide, *Palaeogeogr. Palaeoclim. Palaeoecology*, 97, 151–189, 1992. 1436, 1439, 1444, 1469, 1472

15 Walker, J. C. G., Hays, P. B., and Kasting, J. F.: Negative feedback mechanism for the long-term stabilization of earth's surface temperature, *J. Geophys. Res.*, 86, 9776–9782, 1981. 1444
WOA05: World Ocean Atlas 2005, NOAA Atlas NESDIS 61, available at: http://www.nodc.noaa.gov/OC5/WOA05/pr_woa05.html (last access: 27 June 2011), Washington, DC, 2005. 1457

20 Zachos, J. C., Röhl, U., S. A. Schellenberg, A. S., Hodell, D. A., Kelly, D. C., Thomas, E., M. Nicolo, I. R., Lourens, L. J., McCarren, H., and Kroon, D.: Rapid acidification of the ocean during the Paleocene-Eocene Thermal Maximum, *Science*, 308, 1611–1615, 2005. 1459, 1460

25 Zeebe, R. E.: Where are you heading Earth? (Commentary), *Nat. Geosci.*, 4, in press, 2011. 1455

Zeebe, R. E. and Caldeira, K.: Close mass balance of long-term carbon fluxes from ice-core CO₂ and ocean chemistry records, *Nature Geoscience*, 1, 312–315, doi:10.1038/ngeo185, 2008. 1444, 1455

30 Zeebe, R. E. and Ridgwell, A.: Past changes of ocean carbonate chemistry, in: *Ocean Acidification*, edited by: Gattuso, J.-P. and Hansson, L., Oxford University Press, 2011. 1437, 1461

Zeebe, R. E. and Westbroek, P.: A simple model for the CaCO₃ saturation state of the ocean:

[Title Page](#)[Abstract](#)[Introduction](#)[Conclusions](#)[References](#)[Tables](#)[Figures](#)[Back](#)[Close](#)[Full Screen / Esc](#)[Printer-friendly Version](#)[Interactive Discussion](#)

The “Strangelove”, the “Neritan”, and the “Cretan” Ocean, *Geochem. Geophys. Geosyst.*, 4(12), 1104, doi:10.1029/2003GC000538, 2003. 1443

Zeebe, R. E. and Wolf-Gladrow, D. A.: CO₂ in Seawater: Equilibrium, Kinetics, Isotopes, Elsevier Oceanography Series, Amsterdam, 346 pp., 2001. 1442, 1452

5 Zeebe, R. E. and Zachos, J. C.: Reversed deep-sea carbonate ion basin-gradient during Paleocene-Eocene Thermal Maximum, *Paleoceanogr.*, 22, PA3201, doi:10.1029/2006PA001395, 2007. 1446, 1450, 1453, 1469

Zeebe, R. E., Zachos, J. C., Caldeira, K., and Tyrrell, T.: Oceans: Carbon Emissions and Acidification (in Perspectives), *Science*, 321, 51–52, doi:10.1126/science.1159124, 2008. 1437, 1446, 1456, 1459, 1461, 1475

10 Zeebe, R. E., Zachos, J. C., and Dickens, G. R.: Carbon dioxide forcing alone insufficient to explain Palaeocene-Eocene Thermal Maximum warming, *Nat. Geosci.*, 2, 576–580, doi:10.1038/ngeo578, 2009. 1437, 1446, 1453, 1456, 1458, 1459, 1460, 1461, 1472, 1476

Table 1. Model-architecture and ocean geometry parameters.

Parameter	Symbol	Value ^a	Unit
# Ocean basins	NOC	3 (4)	–
# Ocean tracers	NOCT	varies	–
# Ocean boxes	NB	10 (13)	–
# Atm. tracers	NATM	1 or 2 ^b	–
# Sediment levels	NSD	13	–
# Equations	NEQ	NOCT × NB + NATM + NOC × NSD	–
Total ocean volume	V_{oc}	$1.29 \times 10^{18,c}$	m^3
Total ocean area	A_{oc}	$3.49 \times 10^{14,c}$	m^2
% Area	f_A	26,18,46,10 ^d	%
% Area	f_A	(15,14,52,9,10) ^{e,f}	%
Height L-box ^g	h_L	100	m
Height H-box ^g	h_H	250	m
Height M-box ^g	h_M	900	m

^a Default: modern version, parentheses: P/E-version. ^b 1: CO₂ ; 2: CO₂ and ¹³CO₂. ^c Toggweiler (1999). ^d Atlantic, Indian, Pacific, High-latitude. ^e (Atlantic, Indian, Pacific, Tethys, High-latitude). ^f Bice and Marotzke (2002). ^g L = Low-latitude surface, H = High-latitude surface, M = interMediate.

[Title Page](#)[Abstract](#)[Introduction](#)[Conclusions](#)[References](#)[Tables](#)[Figures](#)[◀](#)[▶](#)[◀](#)[▶](#)[Back](#)[Close](#)[Full Screen / Esc](#)[Printer-friendly Version](#)[Interactive Discussion](#)

[Title Page](#)[Abstract](#)[Introduction](#)[Conclusions](#)[References](#)[Tables](#)[Figures](#)[◀](#)[▶](#)[◀](#)[▶](#)[Back](#)[Close](#)[Full Screen / Esc](#)[Printer-friendly Version](#)[Interactive Discussion](#)**Table 2.** Physical and biogeochemical parameters (ocean model).

Parameter	Symbol	Value ^a	Unit
Conveyor Transport	T	20 ^b (25)	Sv ^c
Upwelling (D–M) ^d	t_A, t_I	0.2, 0.2 ^{e,f}	–
Mixing (L–M) ^d	m_{lk}	21, 17, 25 ^{g,f}	Sv
Mixing (L–M) ^d	m_{lk}	(13, 13, 27, 12) ^{h,f}	Sv
Mixing (H–D) ^d	m_{lk}	4, 3, 10 ^{g,f}	Sv
Mixing (H–D) ^d	m_{lk}	(5, 5, 8) ^{g,f}	Sv
Temperature (initial)	T_C^0	20, 10, 2, 2 ⁱ	°C
Temperature (initial)	T_C^0	(25, 16, 12, 12) ⁱ	°C
Temp. relax. time	τ_n	20, 200, 1000 ^j	yr
Salinity	S	34.7	–
Gas exch. coeff. CO ₂	κ_{as}	0.06 ^k	mol(μatm m ² yr) ⁻¹
Biopump-efficiency	f_{ep1}	0.80 ^f	–
Remin. fraction (M) ^d	f_{rim}	0.78 ^f	–
Remin. fraction (D) ^d	$1 - f_{rim}$	0.22	–
P/C in C _{org}	REDPC	1/130	–
N/C in C _{org}	REDNC	15/130	–
O ₂ /C (C _{org} -remin.)	REDO2C	165/130	–
C-export (H) ^d	F_{eph}	1.8 ^f	mol m ⁻² yr ⁻¹
P-export (H) ^d	F_{pph}	$F_{eph} \times \text{REDPC}$	mol m ⁻² yr ⁻¹
Rain ratio ^l	r_{rain}	6.1 (6.7) ^f	–
CaCO ₃ water dissol. ^m	v_{wc}	0.31 ^f	–

^a Default: modern version, parentheses: P/E-version. ^b Toggweiler (1999). ^c 1 Sv = 10⁶ m³ s⁻¹. ^d L = Low-latitude surface, H = High-latitude surface, M = InterMediate, D = Deep. ^e Fraction upwelled into intermediate Atlantic, Indian (see Figure 2). ^f Tuned. ^g Atlantic, Indian, Pacific. ^h (Atlantic, Indian, Pacific, Tethys). ⁱ L, M, D, H-box. ^j Surface, intermediate, deep. ^k Broecker and Peng (1998). ^l C_{org} : CaCO₃. ^m Fraction of total CaCO₃ export dissolved in water column.

Table 3. Weathering and sediment model parameters.

Parameter	Symbol	Value ^a	Unit
CaCO ₃ weath. flux (initial)	F_{cc}^0	12 ^b (16)	10 ¹² mol yr ⁻¹
CaSiO ₃ weath. flux (initial)	F_{si}^0	5 ^c (6)	10 ¹² mol yr ⁻¹
CO ₂ degass. flux (initial)	F_{vc}^0	F_{si}^0	10 ¹² mol yr ⁻¹
CaCO ₃ weath. exponent	n_{cc}	0.4 ^d	–
CaSiO ₃ weath. exponent	n_{si}	0.2 ^d	–
Height sediment mixed layer	h_s	0.08	m
Density, solids	ρ_s	2.5 × 10 ³	kg m ⁻³
non-CaCO ₃ flux ^e	F_{rrf}	0.35 × 10 ⁻²	kg m ⁻² yr ⁻¹
Porosity, pure clay	ϕ_0	0.85 ^f	–
Porosity, pure CaCO ₃	ϕ_1	0.62 ^f	–
Dissolution rate const. (eff.) ^g	K_{sd}	20.36 × 10 ¹⁰	mol m ⁻² yr ⁻¹
Dissolution rate order (eff.) ^g	n_{sd}	2.40	–

^a Default: modern version, parentheses: P/E-version. ^b Morse and Mackenzie (1990). ^c Walker and Kasting (1992). ^d Uchikawa and Zeebe (2008). ^e Rain of refractory, non-CaCO₃ material to sediments. ^f See Zeebe and Zachos (2007). ^g Effective rate parameters, relating bottom water undersaturation to dissolution rate (Keir, 1982; Sundquist, 1986; Sigman et al., 1998; Zeebe and Zachos, 2007); n_{sd} is not to be confused with the calcite reaction order n , relating porewater undersaturation to dissolution rate (typically $n = 4.5$).

[Title Page](#)[Abstract](#)[Introduction](#)[Conclusions](#)[References](#)[Tables](#)[Figures](#)[◀](#)[▶](#)[◀](#)[▶](#)[Back](#)[Close](#)[Full Screen / Esc](#)[Printer-friendly Version](#)[Interactive Discussion](#)

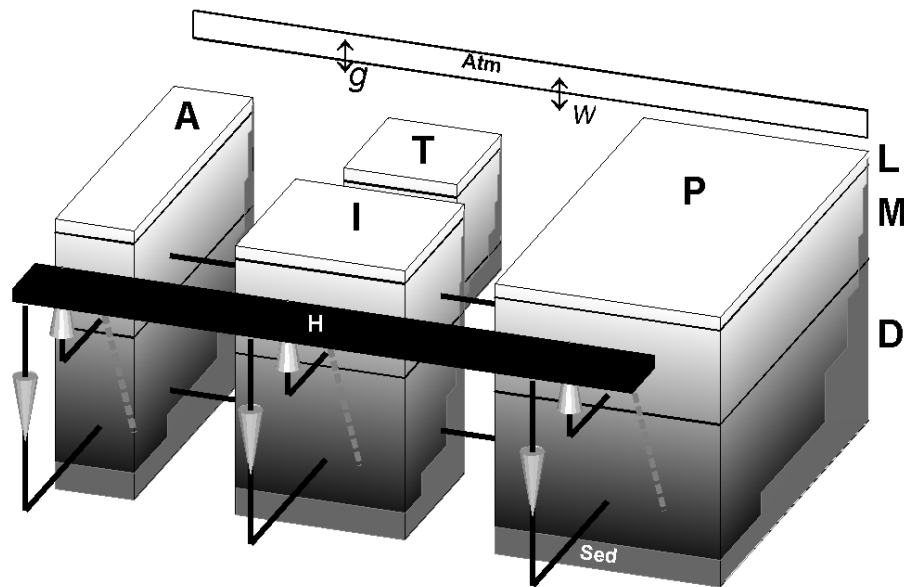


Fig. 1. Schematic representation of the LOSCAR model (Paleocene/Eocene configuration). A = Atlantic, I = Indian, P = Pacific, T = Tethys ocean, H = High-latitude surface, L = Low-latitude surface, M = interMediate, D = Deep box. Weathering fluxes and gas exchange with the atmosphere (Atm) are indicated by “w” and “g”, respectively. Steps on the faces of ocean boxes indicate sediments (Sed).

Title Page

Abstract

Introduction

Conclusions

References

Tables

Figures

◀

▶

◀

▶

Back

Close

Full Screen / Esc

Printer-friendly Version

Interactive Discussion



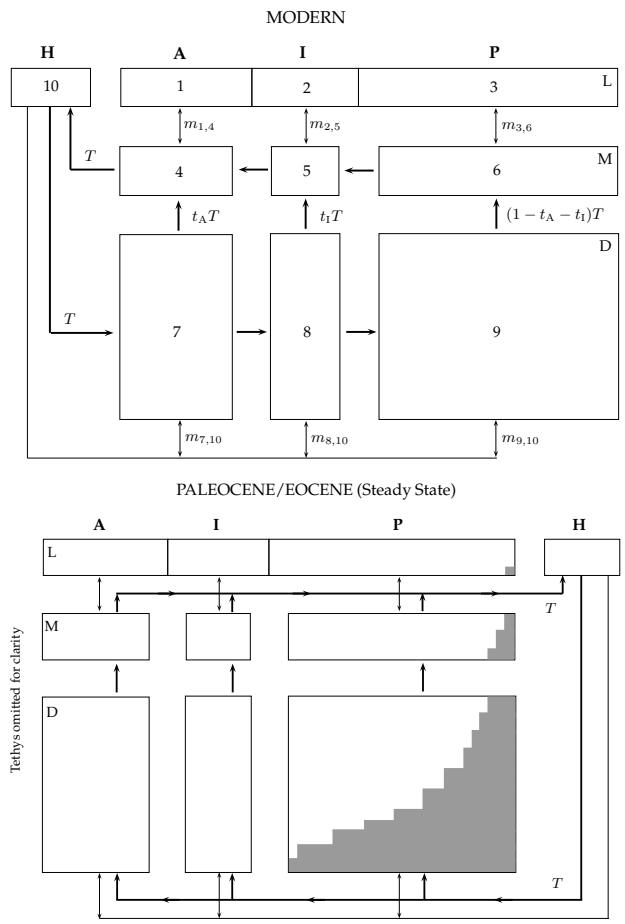


Fig. 2. Caption on next page.

Fig. 2. Ocean circulation and mixing schemes implemented in LOSCAR for modern setup (top) and Paleocene/Eocene (P/E) steady-state (bottom). A = Atlantic, I = Indian, P = Pacific ocean, H = High-latitude surface. In the P/E-setup, the Tethys has been omitted for clarity. L = Low-latitude surface, M = interMediate, D = Deep box. T represents the conveyor transport, while the coefficients m_{lk} represent bidirectional mixing between boxes. The generic H-box represents cold surface waters without reference to a specific location. Nevertheless, the modern setup is motivated by preindustrial circulation patterns with significant deep water formation in the North Atlantic (e.g. Walker and Kasting, 1992; Toggweiler, 1999). The P/E steady-state setup is inspired by observations and modeling studies of Paleocene/Eocene circulation patterns with significant deep water formation in the Southern Ocean (e.g. Bice and Marotzke, 2002; Thomas et al., 2003; Lunt et al., 2010). Note that a transient contribution of North Pacific deep water (not shown) was included in our PETM simulations (Zeebe et al., 2009). All ocean boxes (except H-box) in the modern and P/E-setup are coupled to sediment boxes (schematically indicated only in the bottom panel for the Pacific by the gray shaded area).

[Title Page](#)
[Abstract](#)
[Introduction](#)
[Conclusions](#)
[References](#)
[Tables](#)
[Figures](#)
[Back](#)
[Close](#)
[Full Screen / Esc](#)
[Printer-friendly Version](#)
[Interactive Discussion](#)

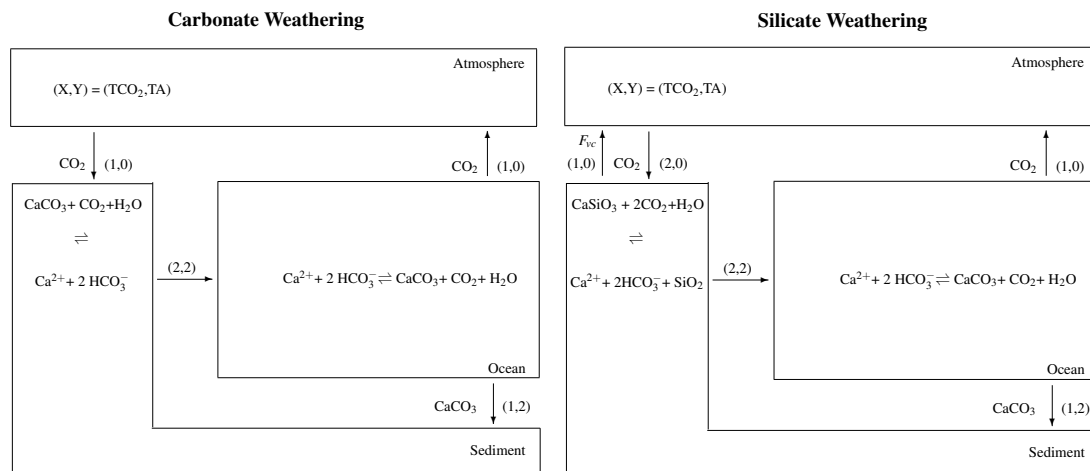



Fig. 3. Schematic illustration of carbonate and silicate weathering fluxes. Numbers in parentheses indicate steady-state fluxes of TCO_2 and TA in mole per mole of $CaCO_3$ or $CaSiO_3$ weathered.

[Title Page](#)
[Abstract](#)
[Introduction](#)
[Conclusions](#)
[References](#)
[Tables](#)
[Figures](#)
[◀](#)
[▶](#)
[◀](#)
[▶](#)
[Back](#)
[Close](#)
[Full Screen / Esc](#)
[Printer-friendly Version](#)
[Interactive Discussion](#)

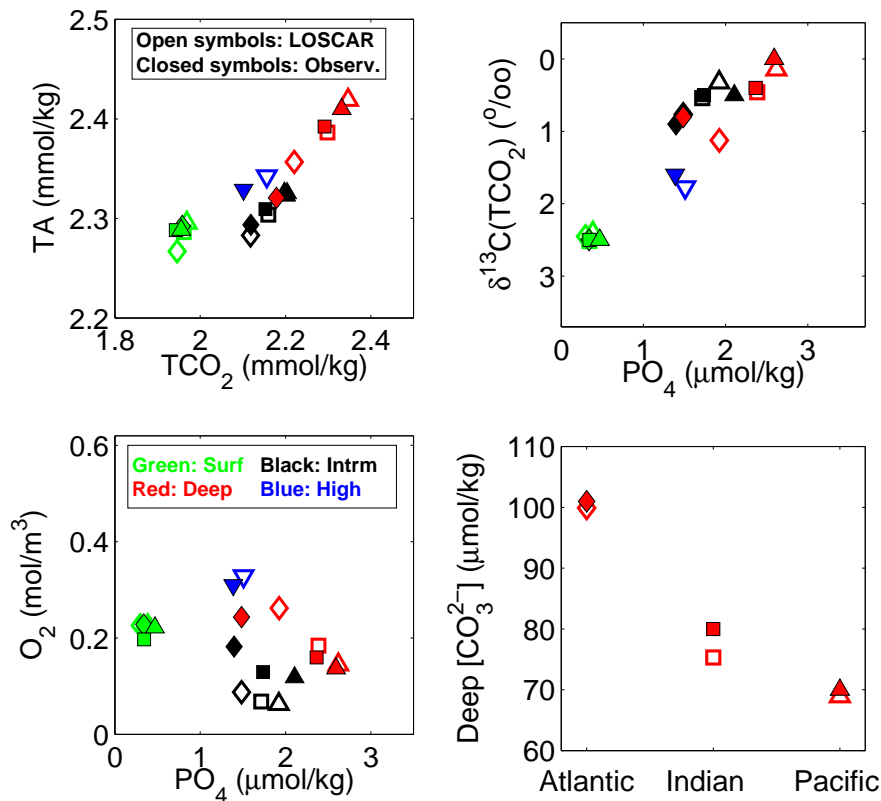



Fig. 4. Computed model tracers and observations used for LOSCAR parameter tuning for modern (preindustrial) configuration, see text for details.

[Title Page](#)

[Abstract](#)

[Introduction](#)

[Conclusions](#)

[References](#)

[Tables](#)

[Figures](#)

[◀](#)

[▶](#)

[◀](#)

[▶](#)

[Back](#)

[Close](#)

[Full Screen / Esc](#)

[Printer-friendly Version](#)

[Interactive Discussion](#)



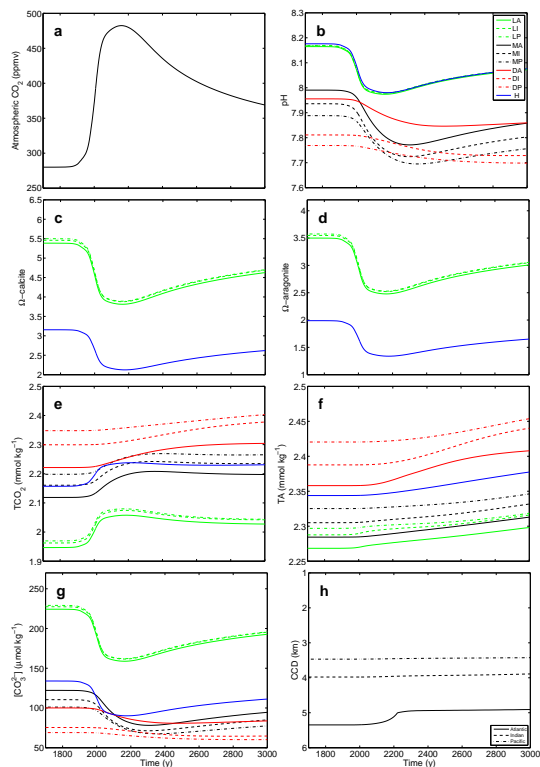


Fig. 5. Example of a fossil fuel emission scenario simulated in LOSCAR: total release of 1000 PgC over 500 years (see Zeebe et al., 2008). Results shown slightly differ from those in Zeebe et al. (2008) because ocean temperature was held constant here for simplicity. L = Low-latitude, M = interMediate, D = Deep, H = High-latitude. A = Atlantic, I = Indian, P = Pacific. Note that the step in the Atlantic calcite compensation depth (CCD, panel h) is due to the spacing of sediment-box depth levels in the model (adding more sediment boxes would make the curve smoother).

Title Page

Abstract

Introduction

Conclusions

References

Tables

Figures



Back

Close

Full Screen / Esc

Printer-friendly Version

Interactive Discussion



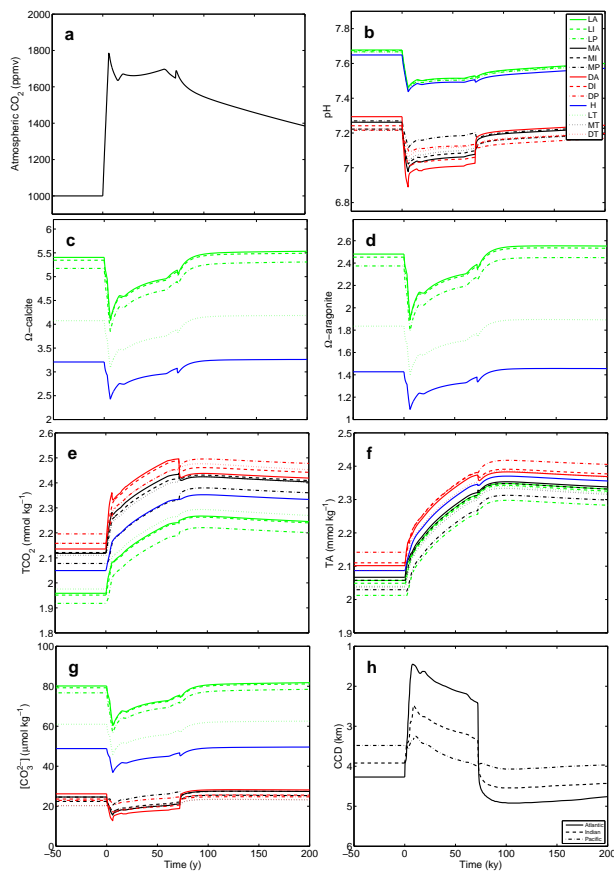


Fig. 6. Example of a PETM carbon release scenario simulated in LOSCAR: initial release of 3000 PgC over a few thousand years (see Zeebe et al., 2009). L = Low-latitude, M = interMediate, D = Deep, H = High-latitude. A = Atlantic, I = Indian, P = Pacific, T = Tethys. See text for details.

[Title Page](#)
[Abstract](#)
[Introduction](#)
[Conclusions](#)
[References](#)
[Tables](#)
[Figures](#)
[Back](#)
[Close](#)
[Full Screen / Esc](#)
[Printer-friendly Version](#)
[Interactive Discussion](#)
